

Active Noise Control for Aircraft Cabin Seats

Ignazio Dimino ^{1,*} , Claudio Colangeli ², Jacques Cuenca ² , Pasquale Vitiello ³ and Mattia Barbarino ³

¹ Adaptive Structures Technologies, The Italian Aerospace Research Centre, Via Maiorise, 81043 Capua, Italy

² Siemens Industry Software NV, Interleuvenlaan 68, 3001 Leuven, Belgium; claudio.colangeli@siemens.com (C.C.); jacques.cuenca@siemens.com (J.C.)

³ Computational Acoustics Laboratory, The Italian Aerospace Research Centre, Via Maiorise, 81043 Capua, Italy; p.vitiello@cira.it (P.V.); m.barbarino@cira.it (M.B.)

* Correspondence: i.dimino@cira.it; Tel.: +39-0823-623308

Abstract: In turboprop aircraft, the low-frequency noise field created by the propellers is the major contributor to the interior vibro-acoustic field, which determines a passenger's discomfort. This paper deals with the experimental assessment of an active noise control (ANC) system for cabin seat headrests using two loudspeakers placed on both sides of the passenger's head to create a local zone of quiet around the passenger's ears. To deal with time-varying disturbances, the developed ANC system utilized a two-input-two-output filtered-X LMS algorithm developed in MATLAB/Simulink and implemented on a DSPACE control board to drive the secondary speakers and cancel the unwanted low-frequency noise components. The performance of the active headrest was investigated through real-time experimentation involving sensors, actuators, and electronic devices. The test results showed that up to approximately 20 dB of sound attenuation could be realized in the passenger's ears over a narrowband sound field replicated under laboratory conditions. Such achievements represent an excellent starting point toward practical applications in the design of more comfortable and acoustically efficient aircraft cabin seats.

Keywords: active noise control; cabin seat; ANC tests; sound intensity map; comfort bubble



Citation: Dimino, I.; Colangeli, C.; Cuenca, J.; Vitiello, P.; Barbarino, M. Active Noise Control for Aircraft Cabin Seats. *Appl. Sci.* **2022**, *12*, 5610. <https://doi.org/10.3390/app12115610>

Academic Editors: Junhong Park and Edoardo Piana

Received: 16 March 2022

Accepted: 30 May 2022

Published: 31 May 2022

Publisher's Note: MDPI stays neutral with regard to jurisdictional claims in published maps and institutional affiliations.



Copyright: © 2022 by the authors. Licensee MDPI, Basel, Switzerland. This article is an open access article distributed under the terms and conditions of the Creative Commons Attribution (CC BY) license (<https://creativecommons.org/licenses/by/4.0/>).

1. Introduction

Active noise control occurs via destructive interference in a given location between a sound field generated by a disturbance source and a controlled secondary source [1]. This technology has proven to be highly effective when dealing with low-frequency noise, and offers multiple benefits in environments where passive treatments are bulky and impractical due to weight penalties [2].

In turboprop aircraft, cabin noise is widely recognized as a major cause of a passenger's discomfort [3]. Low-frequency discrete tones occurring at integer multiples of the blade passing frequency (BPF) dominate the cabin interior noise by affecting passengers' comfort perception during aircraft flight. Practical feedforward controllers, using a multichannel generalization of the well-known LMS adaptive algorithm, have been developed in the literature to reduce the propeller-induced noise in turboprop aircraft cabins [4,5]. After its first application by Morgan [6] and its independent use by Widrow [7], the filtered-X LMS algorithm has been widely used for active noise control applications due to its robustness and simplicity of implementation. Successful experiments were conducted on a Saab 2000 turboprop aircraft by using a number of secondary loudspeakers mounted on the trim panels and at foot level [8]. Nowadays, similar solutions are in service within the Bombardier Q-Series Dash 8 and the Raytheon Beech King Air 350 and are optional for other turboprop and business jet cabins. Similarly, Elliott et al. demonstrated active engine noise control in 1988 [9]. A few years later, the authors extended automotive active control to the road noise control problem [10]. Today, the car industry offers ANC solutions to provide an improved level of interior comfort and driving experience in luxury cars [11].

The effectiveness of active noise cancelling of the primary noise depends upon three physical concepts: spatial extent, frequency bandwidth, and coherence of signal [12]. The majority of ANC applications rely on feedforward control strategies (either pure feedforward or combined with feedback). The feedforward signal is either taken from a specific sensor (usually an accelerometer in active vibration control [13,14] or a microphone in active noise control [15,16]) or extracted from the fundamental disturbance frequency. Additionally, adaptive control strategies are ideal when the primary disturbance acting upon the system becomes time-varying in terms of frequency content, amplitude, and phase. In this case, adaptive filters are used to track these variations and the resulting unknown plants. However, although adaptive control algorithms work well in laboratory conditions, critical issues such as convergence speed, step size tuning, and stability may affect overall system performance and prevent their wide use in practical applications.

Modern active noise control systems take advantage of digital signal processing [17]. The control algorithms are implemented on real-time platforms that support a broad range of controller specifications, data acquisition, and plotting features. The control performance is then assessed by comparing acoustic metrics, mainly sound pressure level (SPL), insertion loss, and sound transmission loss, achieved by comparing the active control versus the original uncontrolled counterpart.

The performance of local active headrest systems has been thoroughly investigated by a number of authors in both tonal and broadband sound fields [18–22]. Additionally, a number of virtual sensing algorithms have been developed to shift the zone of quiet to a virtual sensor located at the observer's ear, as first proposed by Elliott and David [23] and more recently implemented by Xiao et al. [24] by using a laser Doppler vibrometer.

Within the framework of the Clean Sky 2 Airframe ITD, the CASTLE project is aimed at delivering low-noise technologies to improve the cabin acoustic comfort of regional turbo-prop aircraft. ANC is deemed as one of the main KPIs to advance passengers' well-being. This technology is being developed and validated up to Technological Readiness Level (TRL) 4 through dedicated experimental campaigns performed at the component level. Numerical assessments are also envisaged at a full-scale level for a digital aero-vibro-acoustic model of an actual aircraft cabin, including the modeling of both the external disturbances and the primary and secondary components [25–27].

In this paper, the practical implementation of an active headrest system for aircraft cabin seats is presented. The concept is based on the use of a pair of speakers integrated into the headrest of a passenger seat and located on both sides of the passenger's head to attenuate certain low-frequency tonal noise components, thus creating a local zone of quiet (comfort area) around the passenger's ears. The work focuses on the experimental activities executed on a mock-up of a cabin seat equipped with the ANC headrest system to investigate the technological potential of this local noise-cancelling solution in a representative acoustic field. The active noise control logic is implemented on a laboratory DSP control system and associated hardware is tested by simulating the propeller-induced noise of a turboprop aircraft in a reference environment.

2. ANC Headrest System

The zone of quiet in a diffuse sound field has been extensively studied in the literature [28–30]. Elliott et al. [31] investigated the spatial extent of the zone of quiet while controlling pressure with a remote secondary source in a pure tone diffuse sound field. It was defined by a *sinc* function, with the primary sound pressure level attenuated by 10 dB over a region size of about one-tenth of the acoustic wavelength. Elliott and Garcia-Bonito [32] investigated the control of both the pressure and the pressure gradient in a diffuse sound field with two secondary sources. A considerable attenuation of the primary field can be achieved if the primary and secondary sources are positioned within half of a wavelength of each other at the frequency of interest [33].

There are many challenges in developing an ANC headrest system that meets the practical implementation requirements commonly used in aviation. In practical applications,

although the noise levels inside the cabin may be efficiently predicted by simplified vibro-acoustic models, the actual characteristics of noise sources and their vibro-acoustic coupling with the airframe and fuselage lining panels remain uncertain. Computing and hardware costs may be also an issue, especially as a consequence of the limited size and weight margins for instrumentation and control systems onboard. Quiet-Bubble™ technology, developed by Silention Ltd. [34], is an example of one of the most advanced commercial solutions with proven efficiency in the low–medium frequency range. Such a system offers an interesting dB/kg ratio when applied in place of passive NVH systems. This is achieved via a multichannel algorithm that allows control of the sound field produced by an array of counteracting loudspeakers. A detailed description of the control logics can be found in [35]. Other examples include the systems of Ultra Electronics [36], which were successfully tested in a passenger cabin onboard a Saab 2000 in the late 1990s to reduce the fundamental frequency of propeller noise at 97 Hz.

In this study, a dedicated mock-up of a cabin seat equipped with integrated sensors and actuators was investigated to demonstrate the potential of the proposed active noise control concept under laboratory conditions. The secondary loudspeakers were placed at the inner side of the headrest and the error microphones at the end side. The sound pressure was minimized at the physical error signal to create a localized zone of quiet extended to the passenger's ears when the active noise control system was operating. The system was conceived to actively reduce the narrowband periodic noise locally detected by passengers through an active noise canceling function (commonly delivered by active headsets) without the need to wear a headset.

The proposed concept is shown in Figure 1. A pair of speakers was integrated into the seat headrest to create a local comfort area on both sides of the passenger's head, thus improving the passenger's comfort perception. The monitoring microphones were located near the aircraft headrest and used as an error signal to drive the secondary loudspeakers through destructive interference.

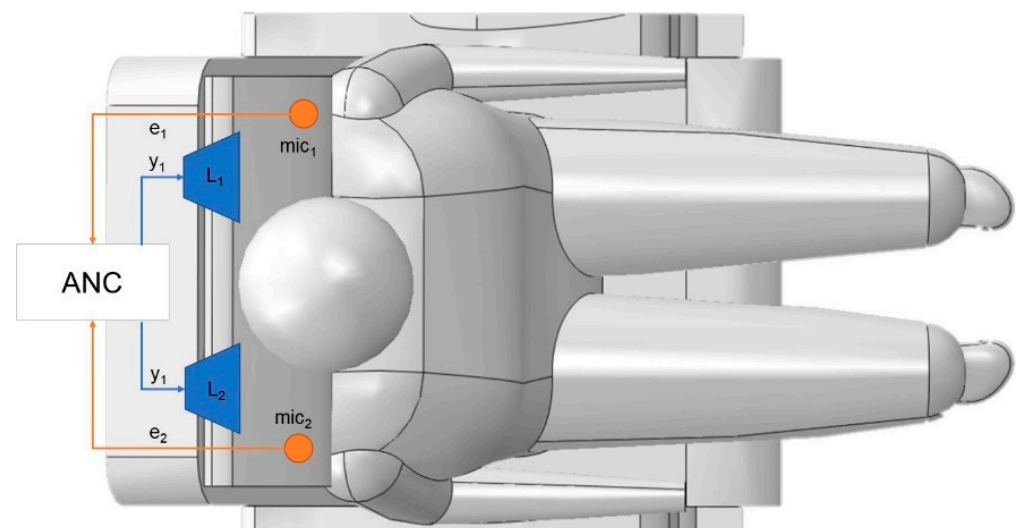


Figure 1. Active noise control from the cabin seat headrest.

Two-Channel ANC Headrest System

In this section, a general block diagram for a multichannel feedforward control is first briefly described. After that, the developed $2 \times 2 \times 2$ ANC headrest system, based on a multiple-input, multiple-output (MIMO) filtered reference least mean squares (FxLMS) algorithm, is presented.

In Figure 2, it is assumed that there are J reference signals, K secondary sources, and M error sensors. Block **S** represents a matrix of $M \times K$ error paths (transfer functions from each secondary source to each error sensor), and block **W** is a matrix of $K \times J$ control filters.

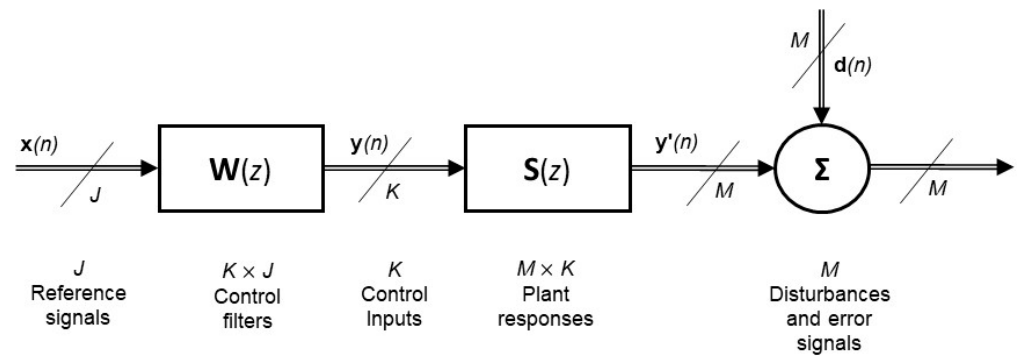


Figure 2. Block diagram of a general multichannel feedforward control with J reference signals, K secondary sources, and M error sensors.

The control signal of the k th secondary source can be expressed as:

$$y_k(n) = \sum_{j=1}^J \mathbf{w}_{kj}^T(n) \mathbf{x}_j(n) \tag{1}$$

where $\mathbf{x}_j(n)$ are the data sequences of the reference signals of length N_w

$$\mathbf{x}_j(n) = [x_j(n) \quad x_j(n-1) \quad \dots \quad x_j(n-N_w+1)]^T \tag{2}$$

and the adaptive filter weights $\mathbf{w}_{kj}(n)$ are defined as follows:

$$\mathbf{w}_{kj}(n) = [w_{kj,1}(n) \quad w_{kj,2}(n) \quad \dots \quad w_{kj,N_w}(n)]^T \tag{3}$$

In this work, a $2 \times 2 \times 2$ feedforward ANC system was implemented by using the adaptive FxLMS algorithm. The structure of the multichannel feedforward ANC headrest system is illustrated in Figure 3. It consists of two reference signals, two loudspeakers (L_1 and L_2), and two error microphones (mic_1 and mic_2) mounted on the headrest. In common with a single channel filtered reference algorithm, the control filter coefficients are iteratively adjusted at every sample time by using a gradient estimate [1].

From (3), the control signals ($y_1(n)$ and $y_2(n)$) fed to the secondary loudspeakers can be calculated as follows:

$$y_1(n) = y_{11}(n) + y_{12}(n) = \mathbf{w}_{11}^T(n) \mathbf{x}_1(n) + \mathbf{w}_{12}^T(n) \mathbf{x}_2(n) \tag{4}$$

$$y_2(n) = y_{21}(n) + y_{22}(n) = \mathbf{w}_{21}^T(n) \mathbf{x}_1(n) + \mathbf{w}_{22}^T(n) \mathbf{x}_2(n) \tag{5}$$

The adaptation equation of the multiple-channel FxLMS reads:

$$\mathbf{w}_{kj}(n+1) = \mathbf{w}_{kj}(n) + \mu \sum_{m=1}^M \mathbf{x}'_{jkm}(n) e_m(n) \tag{6}$$

where the filtered reference signal vector \mathbf{x}'_{jkm} is obtained from linear convolution of the data sequence $\mathbf{x}_j(n)$ and the secondary path estimate \hat{s}_{mk} , which can be obtained by means of system identification using adaptive finite impulse response filters.

The adaptation step size μ controls the convergence properties of the algorithm. It is worth noting that the coefficients of each filter are independently updated by using a weighted combination of the errors at the M sensors.

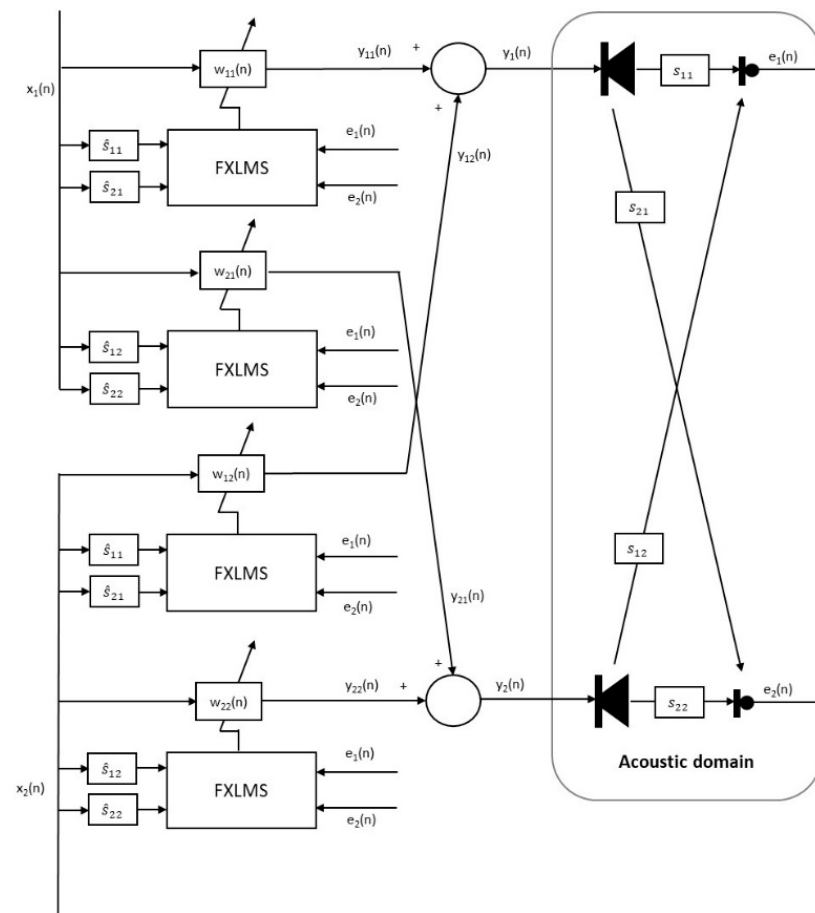


Figure 3. The block diagram of the $2 \times 2 \times 2$ FxLMS algorithm for active noise cancellation of the ANC headrest system.

3. Experimental Set-Up

An experimental campaign was carried out at CIRA to evaluate the proposed technology in laboratory conditions. A set-up consisting of a dummy seat with a headrest was equipped with two monitoring and error microphones and tested within a semi-anechoic chamber. Similar experimental conditions were also investigated in [25] to assess the acoustic performance of two passive noise control concepts based on either a tailored headrest shape or an innovative nanofibrous textile material. The receiving room was a semi-anechoic chamber with dimensions of $6.5 \times 5.3 \times 4.2$ m (volume 145 m^3) and a cut-off frequency of 70 Hz. A binaural head was also used to replicate passenger volume and acquire reliable acoustic data at the position of the ears.

In the laboratory set-up shown in Figure 4, the noise disturbance was generated by a dodecahedral source at 200 Hz. This tonal acoustic field was assumed to replicate the second turboprop harmonics detected by passengers within the cabin as the primary noise field to be cancelled. The free space next to the passenger was an approximation of the cabin environment, whereas the two speakers on the passenger's sides simulated the counteracting noise field. The acoustic acquisitions were made over the entire audible range (20–20,000 Hz). The analysis compared the acoustic field, which was recorded and then elaborated in terms of SPL and sound intensity, with the acoustic control activated and non-activated, at the position of the ears.

The multichannel filtered-x version of the adaptive LMS algorithm was developed in MATLAB/Simulink to derive the optimal control signals driving the control loudspeakers. A C code was then generated in Real-Time Workshop and implemented via a DSP control board for real-time experiments.



Figure 4. ANC tests under semi-anechoic conditions.

A schematic of the experimental set-up is shown in Figure 5. The dodecahedral source emitted the disturbing noise, whereas the counteracting acoustic field was generated by two (left and right) Pioneer TS-G1711I1 17 cm dual-cone (170 Watt) loudspeakers. During all the tests, the microphone signals were conditioned by a PCB 16 channel ICP conditioner. Three types of acoustic sensors were used: two (left and right) $\frac{1}{2}$ " control microphones, two embedded microphones in the binaural head, and one probe for sound intensity measurements. The first couple of microphones provided the error signals processed by the active control system. The second one was used to monitor the ANC performance in terms of sound pressure level reduction.

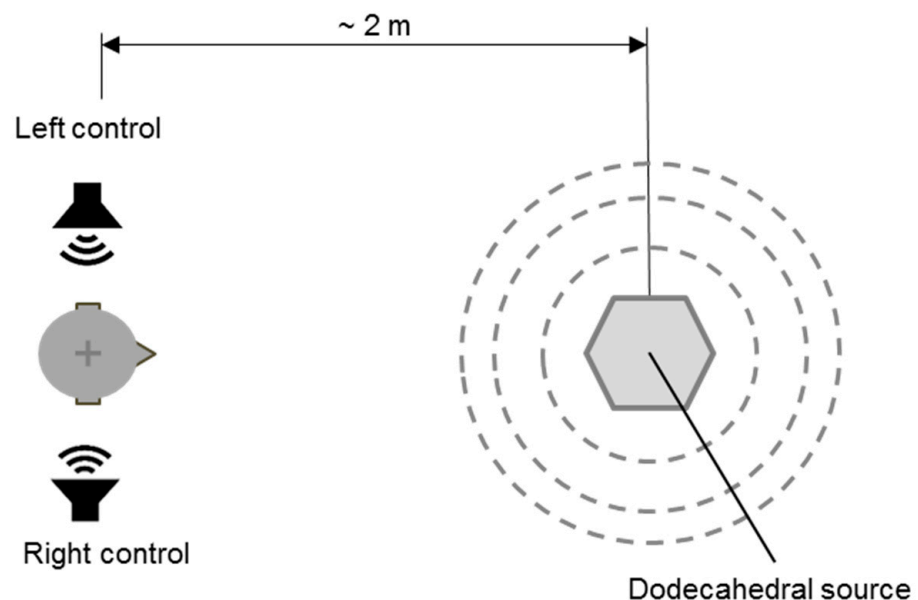


Figure 5. Schematic of the ANC experimental set-up.

Finally, because one of the objectives of the experiments was to assess the dimension of the quiet zones at increasing distances from the passenger, a dedicated probe, shown in Figure 6, was used to map the sound intensity (both magnitude and direction) around the passenger's head.

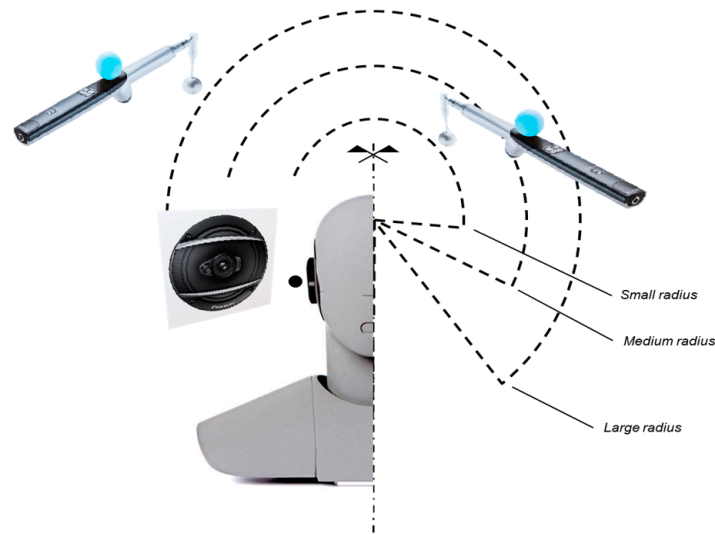


Figure 6. Schematic representation of the concentric spherical surfaces around the binaural head, scanned with the Soundbrush probe.

The sound intensity was measured by a 3D Simcenter Soundbrush system. This acoustic tool combines 3D sound intensity with a visualization of the sound source to provide instant 3D visualization of the sound intensity magnitude and direction during measurements. The acoustic probe contains the data acquisition unit and a color-illuminated sphere so that its position can be determined by a tracking camera, while an inertial platform provides a 3D orientation of the probe. In this way, the system allowed us to measure the sound intensity vectors and map scalar sound pressure amplitudes at multiple circles of varying radii from the same center point. A LMS SCADAS III data acquisition system was also used to measure the acoustic signals and calculate both the primary and secondary FRFs prior to active control system implementation.

A digital dSPACE DS1103 PPC controller board with a real-time processor and a comprehensive I/O was used for control prototyping. The board was mounted on an expansion box to test the control functions within the laboratory set-up. The control and acquisition chains are detailed in Figure 7. All the programs used to acquire data and implement the controllers were developed by using Real-Time Workshop.

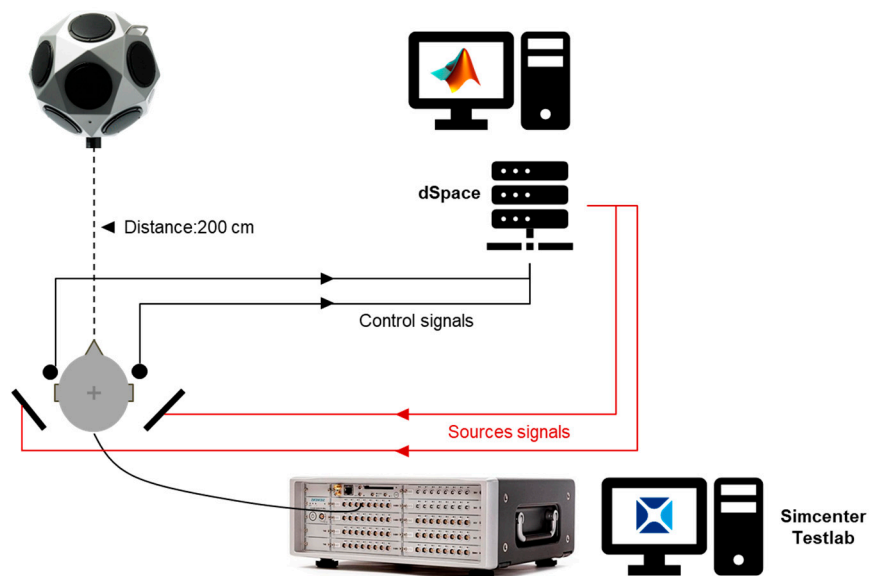


Figure 7. Block diagram of the control and acquisition chains.

4. Experimental Results

Before applying the control, a reference acoustic field acting on the selected passenger’s area was experimentally evaluated. The excitation level was set to about 80 dB in order to reproduce a realistic noise level as detected by passengers within an actual aircraft cabin. By assuming that the off-line identified plants were accurate enough to represent the behavior of the secondary paths, the real-time levels of noise were measured and compared with and without control.

Firstly, after recording acoustic signals for the uncontrolled case, the ANC headrest system was separately invoked for the left and right head positions. The control system capabilities for adaptively attenuating the primary acoustic field were experimentally assessed on the two microphones located left and right of the binaural head. The results are shown in Figure 8. The SPLs measured at the left and right microphones were reduced by approximately 13 dB (left) and 9.5 dB (right), respectively, when only one of the two speakers was alternatively activated. After that, when both controllers were activated, a higher noise attenuation of 19.92 dB (left mic) and 17.36 dB (right mic) was achieved. The noise attenuation results are summarized in Table 1.

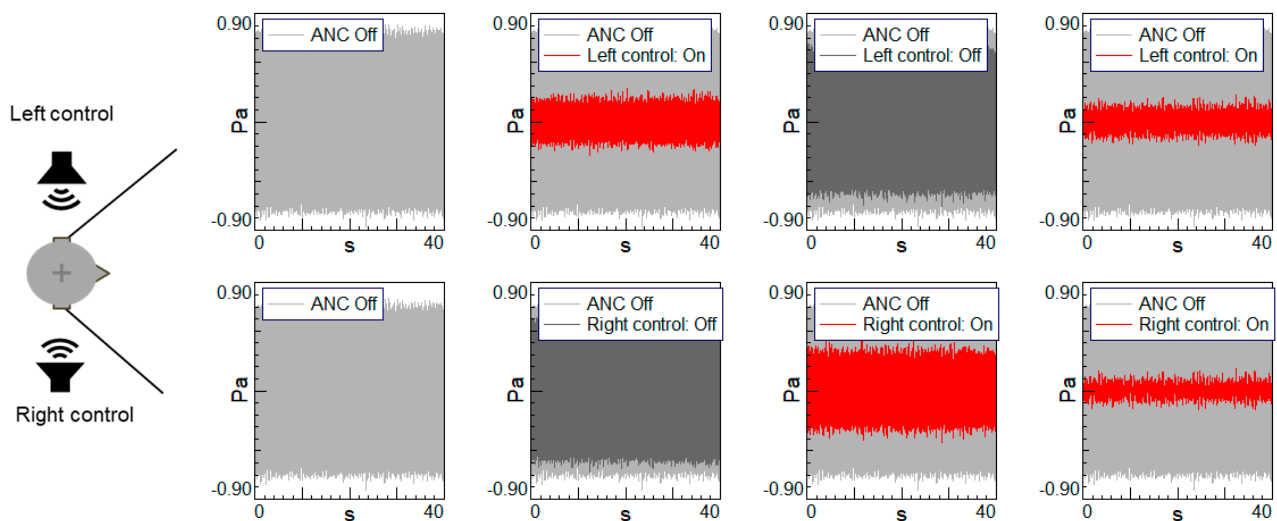


Figure 8. Acoustic signals with/without ANC at left and right mics.

Table 1. Sound pressure levels (SPLs) at left and right ears of the binaural head when using ANC.

	L and R: OFF	L: ON, R: OFF	L: OFF, R: ON	L: ON, R: ON
Left SPL (dB)	88.13 dB	75.02 (−13.11 dB)	88.09 (−0.04 dB)	68.21 (−19.92 dB)
Right SPL (dB)	87.70 dB	86.43 (−1.27 dB)	78.28 (−9.42 dB)	70.17 (−17.36 dB)

Sound intensity measurements were also carried out in the semi-anechoic chamber with and without control in order to characterize the sound power attenuation achieved by the ANC system. Regions with higher sound intensity were interpreted as locations of major perceived sound level. The active and reactive intensity levels were measured by manually scanning a region through concentric spherical surfaces around the binaural head. Figure 9 shows the sound intensity measured on the headrest area with and without controller operation. The local sound intensity map with the control reached a peak of 77 dB in correspondence with the loudspeakers. It was found that a quieter area with a volume of $0.35 \times 0.40 \times 0.5$ m was generated around the binaural head (Figure 10) when the ANC system was activated. Red lobes in the vicinity of the control speakers were also visible, as well as the transition to the quiet zone before reaching the ears of the binaural head.

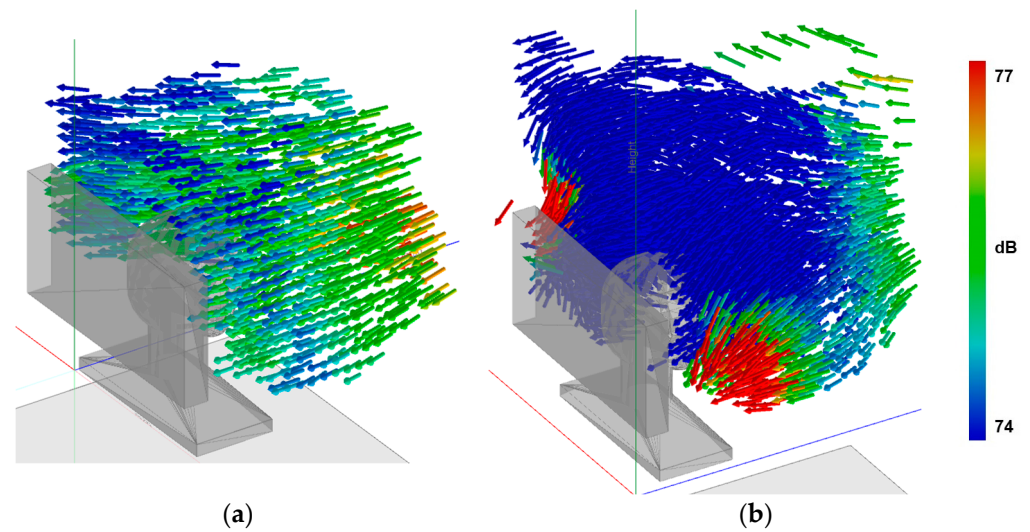


Figure 9. Sound intensity (W/m^2) measured with and without ANC at left and right mics. (a) Sound intensity map without control. (b) Sound intensity map with control.

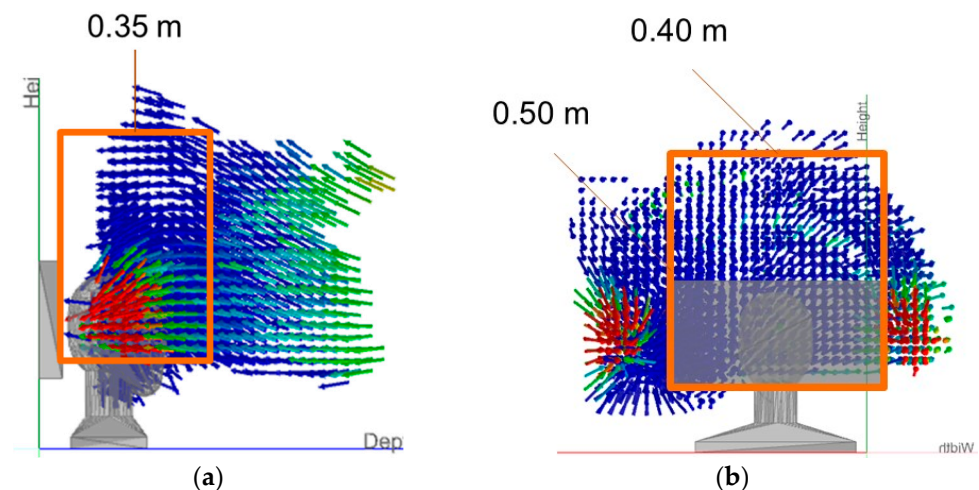


Figure 10. Quiet zone around the passenger's head by ANC. (a) Side view. (b) Front view.

5. Discussion

The variation in the noise reduction performance provided by the developed ANC headrest system was relatively low (below 5%), and the dimension of the comfort bubble was seemingly suitable for practical system implementation. This achievement, which was typically dependent upon the frequency components of the acoustic signal being cancelled, was verified in the course of the experiments. However, one has to consider possible changes in the acoustic paths associated with the ANC system due to the passenger's head movement, which were not addressed in this work. The exact impact of this assumption cannot be clarified yet and requires more research.

The disturbing noise field was simulated by artificially generating tonal and narrow-band disturbances, replicating the propeller-induced noise within a reference test environment under stationary and transient conditions. The primary noise was played through a dedicated speaker placed in front of the mannequin. The system's effectiveness was validated using representative experiments on local active noise control under laboratory conditions, utilizing a conventional FxLMS algorithm for multi-channel application. The upstream reference signals were taken from the predicted primary narrowband noise acting on the cabin passenger areas where seats are located, which was assumed to be detectable by reference sensors that are not affected by the control field.

However, the proposed approach was restricted to the active control of periodic or nearly periodic noise, which is very common in turboprop aircraft cabins. The accuracy of the amplitude and phase of the secondary sound field generated by the developed signal processing algorithm affected the noise reduction levels, which were different for the left and right ears when the two speakers were alternatively activated. The control performance observed at the two microphones was also slightly different when the two speakers were simultaneously activated.

In summary, our results demonstrated that significant noise reductions can be achieved around a passenger's ears with reasonable spatial variability. However, it is worth noting that, although very promising, these sound attenuations were achieved within free-field conditions (semi-anechoic conditions), thus neglecting the typical standing waves and reflections occurring in actual aircraft cabins. Furthermore, it was tacitly assumed that broadband aerodynamic noise could be separately addressed by using conventional passive techniques. For this reason, an extensive study ahead of system implementation, which considers broadband components up to 500 Hz of interest for the actual operation, is recommended.

6. Conclusions

A study on an ANC headrest system mock-up was conducted to qualify the effectiveness of signal processing algorithms and the related implementation techniques for successful application onboard regional aircraft cabin seats. Although physical implementation constraints and economic considerations were not addressed in the present study, the proposed concept showed efficiency in attenuating low-frequency noise in a controlled environment that replicated the turboprop harmonics of a regional aircraft cabin. The ANC scheme uses two secondary actuators (e.g., loudspeakers) to generate a secondary sound field and two error sensors (e.g., microphones) to pick up residual noise, which serves as the error signal for updating the adaptive filters. A head mannequin equipped with two microphones was used to measure the noise reduction. The results showed that the ANC headrest system achieved sound level reduction of up to 19.92 dB and 17.36 dB at the mannequin's left and right ears, respectively, while the error microphones were placed at the headrest. These moderate but realistic achievements were obtained under free-field conditions (semi-anechoic conditions) by using a representative active seat arrangement. Sound intensity measurements showed an artificial comfort zone of about $0.35 \times 0.40 \times 0.5$ m around the passenger's head. This volume could be considered large enough to include both the lateral and vertical head movements of a passenger, who would therefore be able to benefit from the active noise cancelling system without the need to wear an active headset.

Our experimental activities fully demonstrated the technical feasibility of the proposed concept, opening the way for possible upscaling to TRL5 in a real cabin demonstrator. However, implementation considerations such as system complexity, physical constraints, and cost reduction may affect the system's performance in practical applications. Furthermore, ANC systems on adjacent seats may induce instabilities. Although the ANC system provides promising benefits in terms of overall noise reduction, these benefits cannot be realized without causing a significant fuselage weight increase due to the massive equipment, actuators, and sensors integrated into the cabin seats.

A comparison with other methods used in experimental and some rare commercial systems will be made in future studies. Virtual sensing methods will also be investigated to reposition the point of cancellation and thus increase the upper frequency of control by using head tracking to monitor the passenger's head movement. Numerical optimizations are also envisaged to predict active noise control capabilities at the cabin level and compare them with the experimental data obtained within the project for passive noise control solutions.

Author Contributions: Conceptualization, I.D.; methodology, I.D.; software, I.D.; validation, I.D. and P.V.; formal analysis, I.D. and C.C.; investigation, I.D., C.C. and J.C.; resources, C.C. and J.C.; data curation, M.B.; writing—original draft preparation, I.D.; writing—review and editing, I.D. and J.C.; visualization, I.D.; supervision, I.D.; project administration, M.B.; funding acquisition, M.B. All authors have read and agreed to the published version of the manuscript.

Funding: The research leading to these results was developed within the framework of CASTLE (cabin systems design toward passenger wellbeing) Core Partnership of the Clean Sky 2 Program. CASTLE received funding from the Clean Sky 2 Joint Undertaking under the European Union's Horizon 2020 research and innovation program under the grant agreement no. CS2-AIR-GAM-2014-2015-01. The contents of this paper reflect only the authors' views, and the Clean Sky 2 Joint Undertaking and the European Commission are not liable for any use that may be made of the information contained therein.

Institutional Review Board Statement: Not applicable.

Informed Consent Statement: Not applicable.

Data Availability Statement: Not applicable.

Conflicts of Interest: The authors declare no conflict of interest.

Nomenclature

ITD	Integrated Technology Demonstrator
CASTLE	CS2 Castle project
TRL	Technological Readiness Level
KPI	Key Performance Indicator
CIRA	The Italian Aerospace Research Centre
DSP	Digital Signal Processing
TITO	Two-Input, Two-Output system
FRF	Frequency Response Function
FxLMS	Filtered-x Least Mean Square

References

- Nelson, P.A.; Elliott, S.J. *Active Control of Sound*; Academic Press: Cambridge, MA, USA, 1993.
- Tokhi, M.O.; Veres, S. *Active Sound and Vibration Control—Theory and Applications*; The Institution of Electrical Engineers: London, UK, 2002.
- Dimino, I.; Aliabadi, M.H.F. *Active Control of Aircraft Cabin Noise*; Imperial College Press: London, UK, 2015.
- Nelson, P.A.; Elliott, S.J. Multi-channel adaptive filters for the reproduction and active control of sound fields. In Proceedings of the IEEE ASSP Workshop on Applications of Signal Processing to Audio and Acoustics, New York, NY, USA, 1989.
- Dimino, I.; Vigliotti, A.; Aliabadi, M.H.F.; Concilio, A. Vibro-acoustic design of an aircraft-type active window. Part 1: Dynamic modelling and experimental validation. *J. Theor. Appl. Mech.* **2012**, *50*, 169–192.
- Morgan, D.R. An analysis of multiple correction cancellation loops with a filter in the auxillary path. *IEEE Trans. Speech Signal Processing* **1980**, *ASSP-28*, 454–467. [[CrossRef](#)]
- Widrow, B.; Shur, D.; Shaffer, S. On adaptive inverse control. In Proceedings of the 15th ASILOMAR Conference on Circuits, Systems and Computers, Pacific Grove, CA, USA, 9–11 November 1981; pp. 185–195.
- Johansson, S. Active Control of Propeller-Induced Noise in Aircraft. Ph.D. Thesis, Blekinge Institute of Technology, Ronneby, Sweden, 2000.
- Elliott, S.J.; Stothers, I.M.; Nelson, P.A.; McDonald, A.M.; Quinn, D.C.; Saunders, T. The active control of engine noise inside cars. *Proc. Internoise* **1988**, *88*, 987–990.
- Sutton, T.J.; Elliott, S.J.; McDonald, A.M.; Saunders, T.J. The active control of road noise inside vehicles. *Noise Control Eng. J.* **1994**, *42*, 137–147. [[CrossRef](#)]
- Mackay, A.C.; Kenchington, S. Active control of noise and vibration—A review of automotive applications. In Proceedings of the INTER-NOISE and NOISE-CON Congress and Conference, Williamsburg, VA, USA, 2–6 May 2004.
- Kidner, M.R.F. Active noise control: A review in the context of the cube of difficulty. *Acoust. Aust.* **2006**, *34*, 65–69.
- Magliacano, D.; Viscardi, M.; Ciminello, M.; Dimino, I.; Concilio, A. Feasibility study for a tonal vibration control system of a mounting bracket for automotive gearboxes. *Int. J. Mech.* **2016**, *10*, 403–410.

14. Magliacano, D.; Viscardi, M.; Dimino, I.; Concilio, A. Active vibration control by piezoceramic actuators of a car floor panel. In Proceedings of the ICSV 2016—23rd International Congress on Sound and Vibration: From Ancient to Modern Acoustics, Athens, Greece, 10–14 July 2016; International Institute of Acoustics and Vibrations: Auburn, AL, USA, 2016; pp. 3382–3389, ISBN 9789609922623.
15. Yuanand, J.; Fung, K.-Y. A traveling wave approach to active noise control in ducts. *J. Sound Vib.* **1999**, *219*, 307–321.
16. Lau, S.K.; Tang, S.K. Sound fields in a slightly damped rectangular enclosure under active control. *J. Sound Vib.* **2000**, *238*, 637–660. [[CrossRef](#)]
17. Elliott, S.J. *Signal Processing for Active Control*; Academic Press: Cambridge, MA, USA, 2001.
18. Elliott, S.J.; Jones, M. An active headrest for personal audio. *J. Acoust. Soc. Am.* **2006**, *119*(Pt. 1), 2702–2709. [[CrossRef](#)]
19. Pawelczyk, M. Adaptive noise control algorithms for active headrest system. *Control. Eng. Pract.* **2004**, *12*, 1101–1112. [[CrossRef](#)]
20. Rafaely, B.; Elliott, S.; Garcia-Bonito, J. Broadband performance of an active headrest. *J. Acoust. Soc. Am.* **1999**, *106*, 787–793. [[CrossRef](#)] [[PubMed](#)]
21. Ghebreyesus, W.; Xi, F. Zone Based Active Noise Control via Head Tracking for an Aircraft Seat. In Proceedings of the 9th International Symposium on Fluid-Structure Interactions, Flow-Sound Interactions, Flow-Induced Vibration & Noise, Toronto, ON, Canada, 8–11 July 2018.
22. Siswanto, A.; Chang, C.; Kuo, S.M. Active noise control for headrests. In Proceedings of the 2015 Asia-Pacific Signal and Information Processing Association Annual Summit and Conference (APSIPA), Hong Kong, China, 16–19 December 2015; pp. 688–692. [[CrossRef](#)]
23. Elliott, S.; David, A. A virtual microphone arrangement for local active sound control. In Proceedings of the 1st International Conference on Motion and Vibration Control, Yokohama, Japan, 7–11 September 1992; pp. 1027–1031.
24. Xiao, T.; Qiu, X.; Halkon, B. Ultra-broadband local active noise control with remote acoustic sensing. *Sci. Rep.* **2020**, *10*, 20784. [[CrossRef](#)] [[PubMed](#)]
25. Giannella, V.; Colangeli, C.; Cuenca, J.; Citarella, R.; Barbarino, M. Experimental/Numerical Acoustic Assessment of Aircraft Seat Headrests Based on Electrospun Mats. *Appl. Sci.* **2021**, *11*, 6400. [[CrossRef](#)]
26. Barbarino, M.; Vitiello, P.; Lombardi, R.; Pagano, A. Optimized Synchrophasing System of a Turbo-Prop Aircraft for Cabin Noise Reduction. In Proceedings of the INTERNOISE Conference 2019. Available online: http://www.sea-acustica.es/fileadmin/INTERNOISE_2019/Fchrs/Proceedings/1759.pdf (accessed on 16 March 2022).
27. Galasso, B.; Concilio, A.; Ameduri, A.; Dimino, I.; Vitiello, P.; Barbarino, M. Design of an Adaptive Dynamic Vibration Absorber for Ucoustic Uevels reduction of a Uegional Uircraft Uassengers 'Uabin. In Proceedings of the INTERNOISE Conference 2019. Available online: http://www.sea-acustica.es/fileadmin/INTERNOISE_2019/Fchrs/Proceedings/1645.pdf (accessed on 16 March 2022).
28. Rafaely, B. Zones of quiet in a broadband diffuse sound field. *J. Acoust. Soc. Am.* **2001**, *110*, 296–302. [[CrossRef](#)]
29. Joseph, P.; Elliott, S.J.; Nelson, P.A. Near field zones of quiet. *J. Sound Vib.* **1994**, *172*, 605–627. [[CrossRef](#)]
30. Elliott, S.J.; Cheer, J. Modeling local active sound control with remote sensors in spatially random pressure fields. *J. Acoust. Soc. Am.* **2015**, *137*, 1936–1946. [[CrossRef](#)] [[PubMed](#)]
31. Elliott, S.; Joseph, P.; Bullmore, A.; Nelson, P. Active cancellation at a point in a pure tone diffuse sound field. *J. Sound Vib.* **1988**, *120*, 183–189. [[CrossRef](#)]
32. Elliott, S.; Garcia-Bonito, J. Active cancellation of pressure and pressure gradient in a diffuse sound field. *J. Sound Vib.* **1995**, *186*, 696–704. [[CrossRef](#)]
33. Nelson, P.A.; Elliott, S.J. The minimum power output of a pair of free field monopoles. *J. Sound Vibrat.* **1986**, *105*, 173–178. [[CrossRef](#)]
34. Available online: <https://www.silentium.com/technology-2/quiet-bubble/> (accessed on 11 March 2022).
35. Available online: <http://www.freepatentsonline.com/y2012/0288110.html> (accessed on 11 March 2022).
36. Available online: <https://www.ultra-pcs.com/wp-content/uploads/2017/06/Brochure-noise-control.pdf> (accessed on 11 March 2022).